Electronic Supplementary Information (ESI) for:

Photoinduced electron transfer (PET) *versus* excimer formation in supramolecular p/n-heterojunctions of perylene bisimide dyes and implications for organic photovoltaics

Agnieszka Nowak-Król,[a] Benjamin Fimmel,[a] Minjung Son,[b] Dongho Kim,*[,b] and Frank Würthner*[,a]

[a] Institut für Organische Chemie & Center for Nanosystems Chemistry, Universität Würzburg, Am Hubland, 97074 Würzburg, Germany

[b] Spectroscopy Laboratory for Functional π-Electronic Systems and Department of Chemistry, Yonsei University, Seoul 120-749, Korea

E-mail: wuerthner@chemie.uni-wuerzburg.de, dongho@yonsei.ac.kr

Table of Contents

1. Square Wave Voltammetry

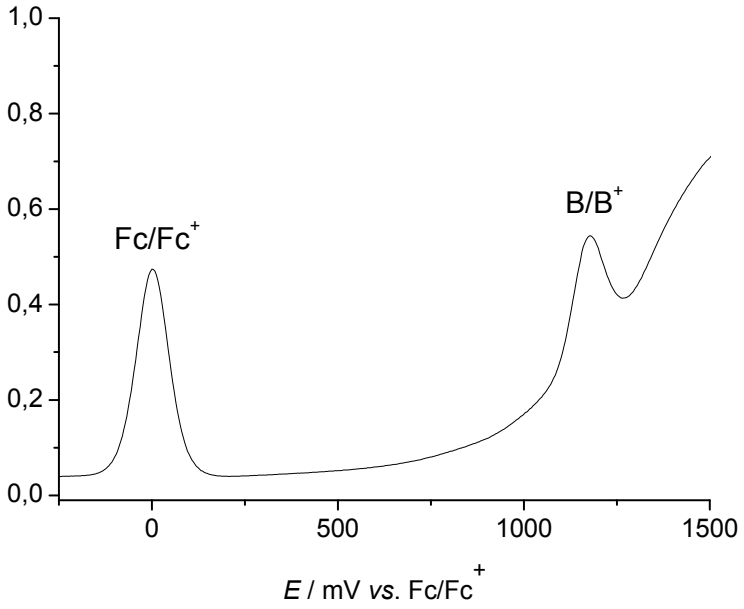

Fig. S1 Square wave voltammogram of **B** in CH_2Cl_2, supporting electrolyte Bu_4NPF_6, internal reference: ferrocene/ferrocenium, scan rate 100 mV s^{-1}.

2. Further Steady-State Absorption and Fluorescence Spectroscopy

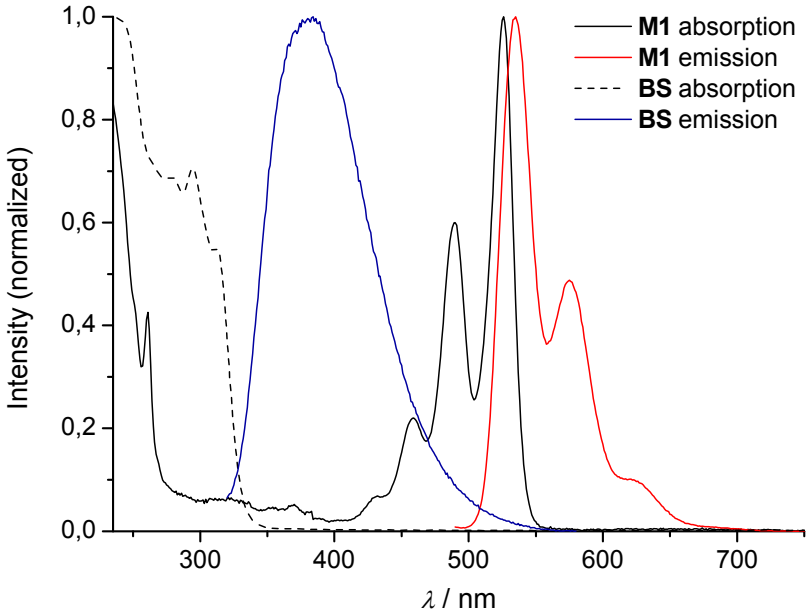

Fig. S2 Normalized absorption and fluorescence emission spectra of **M1** and **BS** in CH_2Cl_2.

3. Time-Resolved Fluorescence Spectroscopy

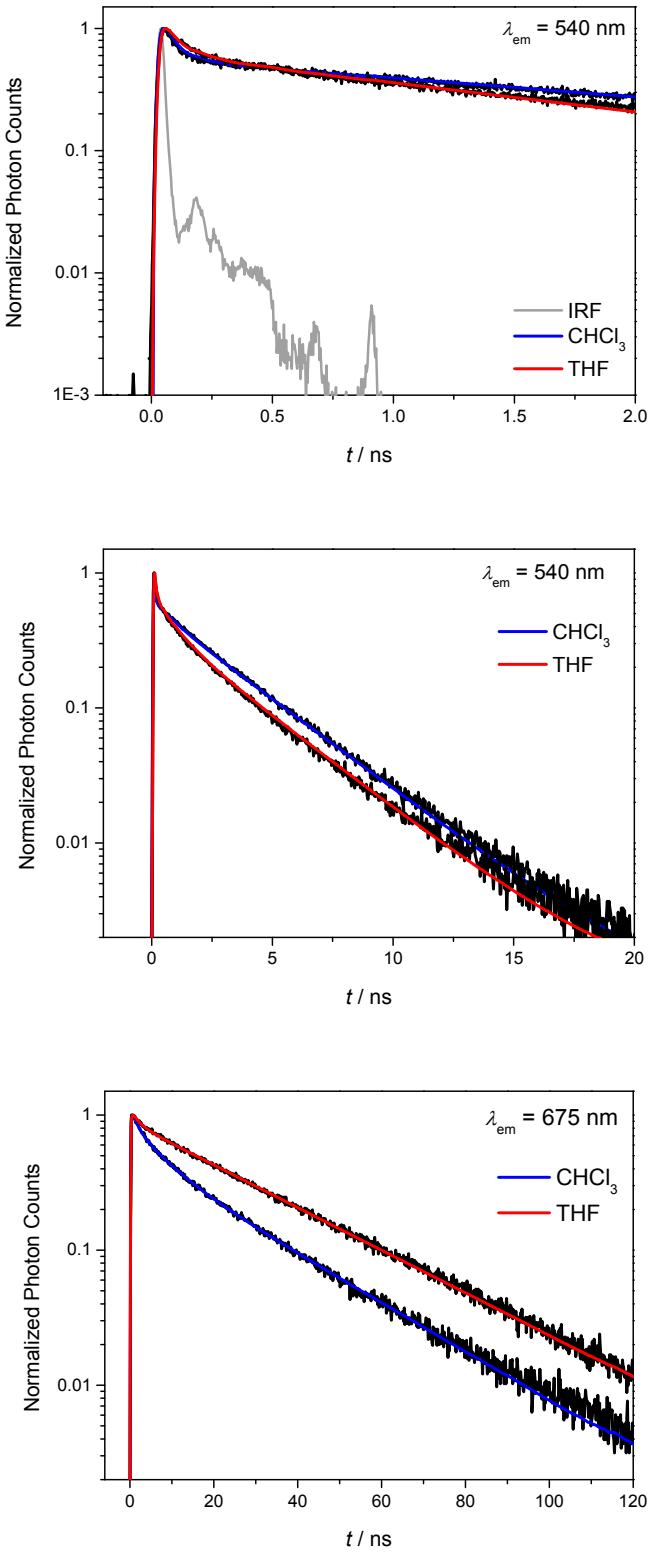

Fig. S3 Time-resolved fluorescence decay profiles of **F2S** (blue fitted lines: in chloroform, red fitted lines: in THF) monitored at 540 nm (top and middle) and 675 nm (bottom), respectively. The instrumental response function (IRF) is shown as the grey trace.

4. Additional Transient Absorption Spectroscopy

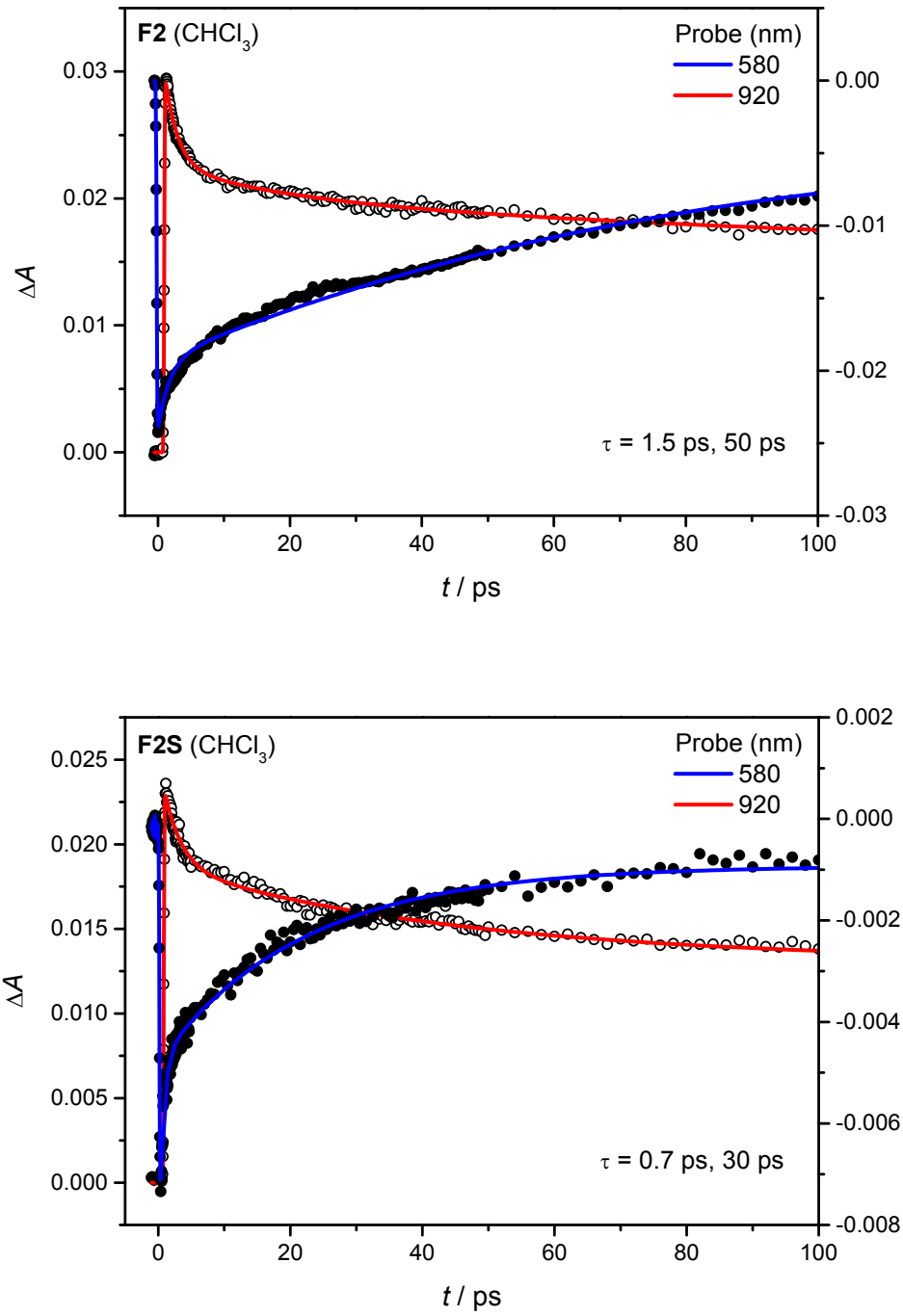

Fig. S4 Transient absorption decay profiles of **F2** and **F2S** in $CHCl_3$. The probe wavelengths employed and fitted time constants are indicated inside each figure.

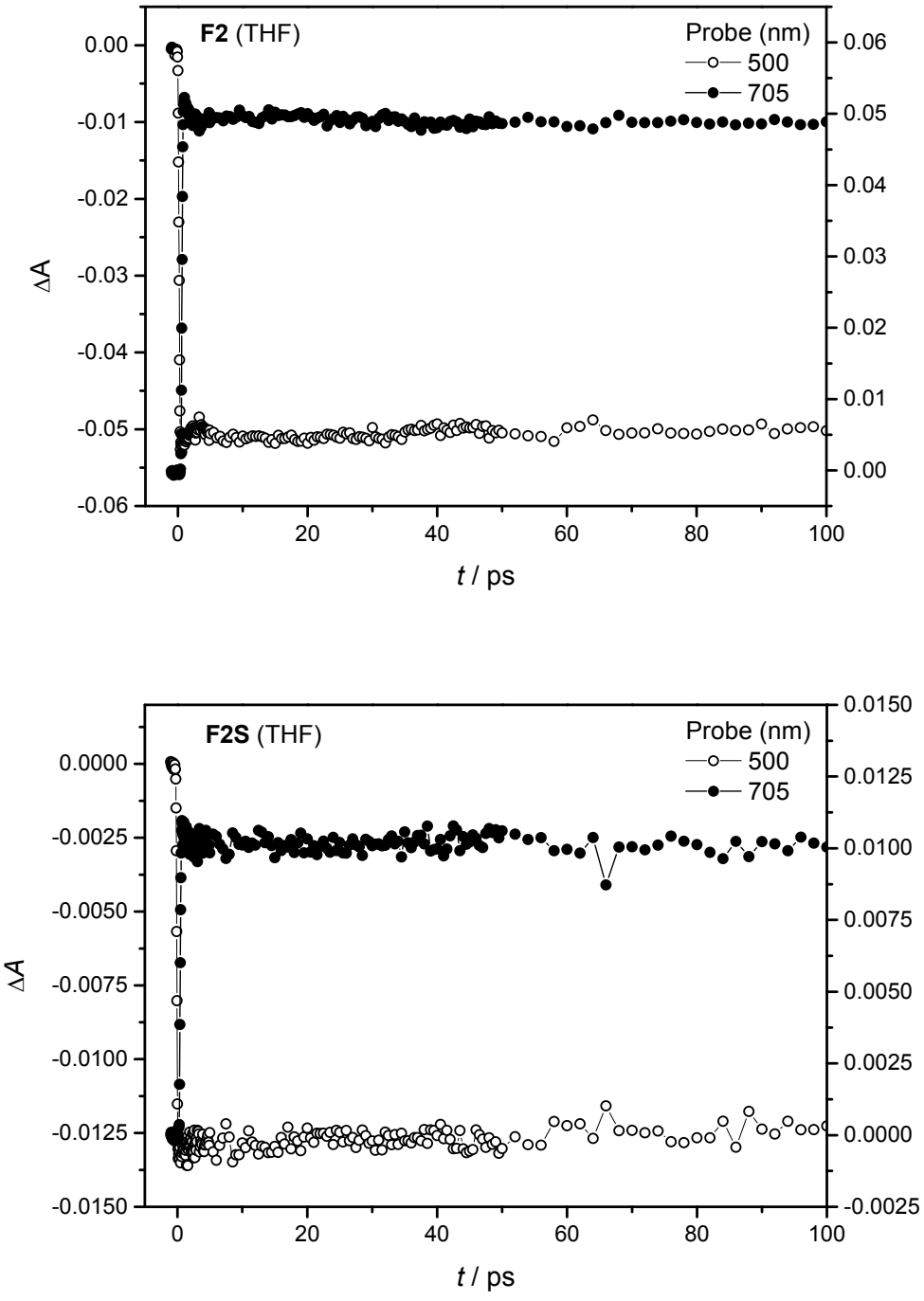

Fig. S5 Transient absorption decay profiles of **F2** and **F2S** in THF. The probe wavelengths employed are indicated inside each figure.

5. NMR and MS Spectra

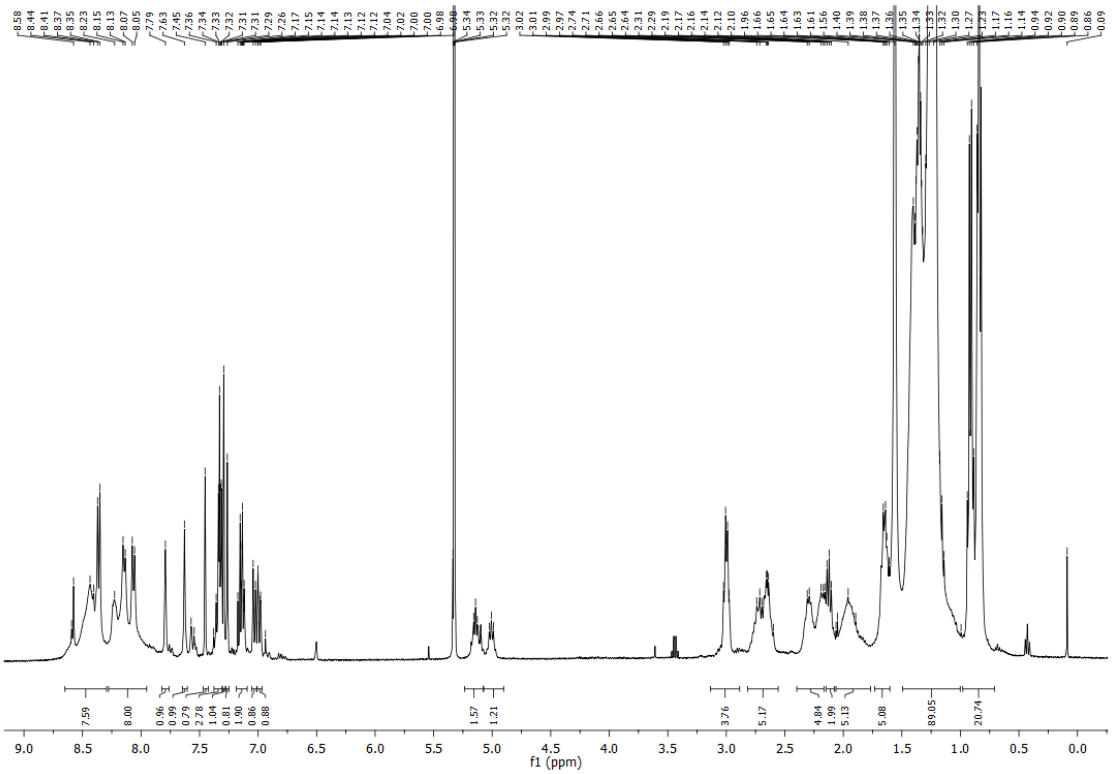

Fig. S6 ^{1}H NMR spectrum of compound **F2S** (400 MHz, CD_2Cl_2, 25 °C).

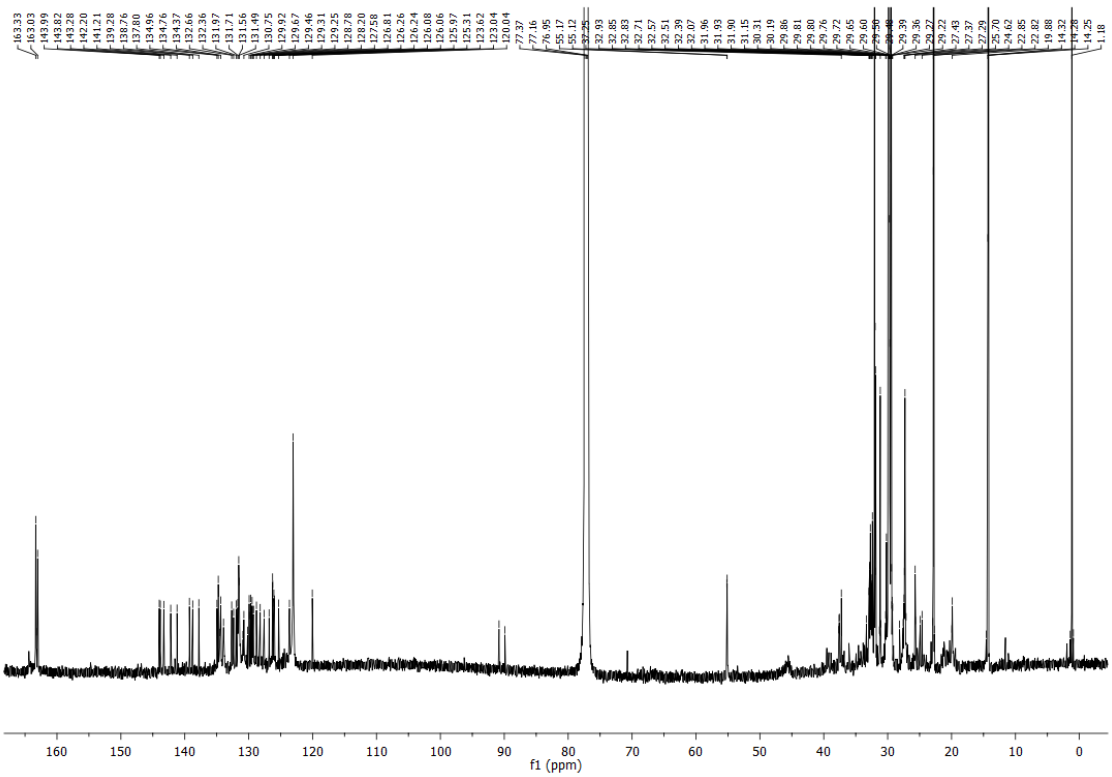

Fig. S7 ^{13}C NMR spectrum of compound **F2S** (151 MHz, $CDCl_3$, 25 °C).

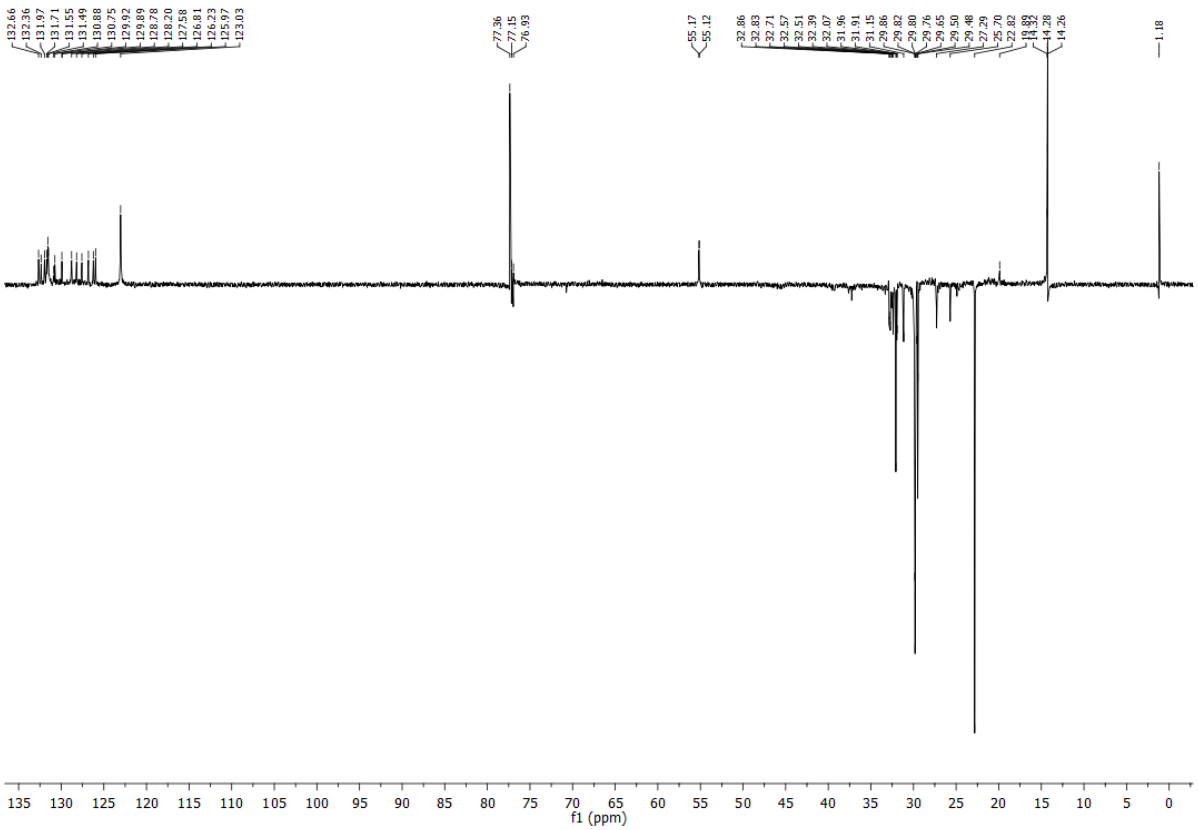

Fig. S8 DEPT-135 spectrum of compound **F2S** (151 MHz, $CDCl_3$, 25 °C).

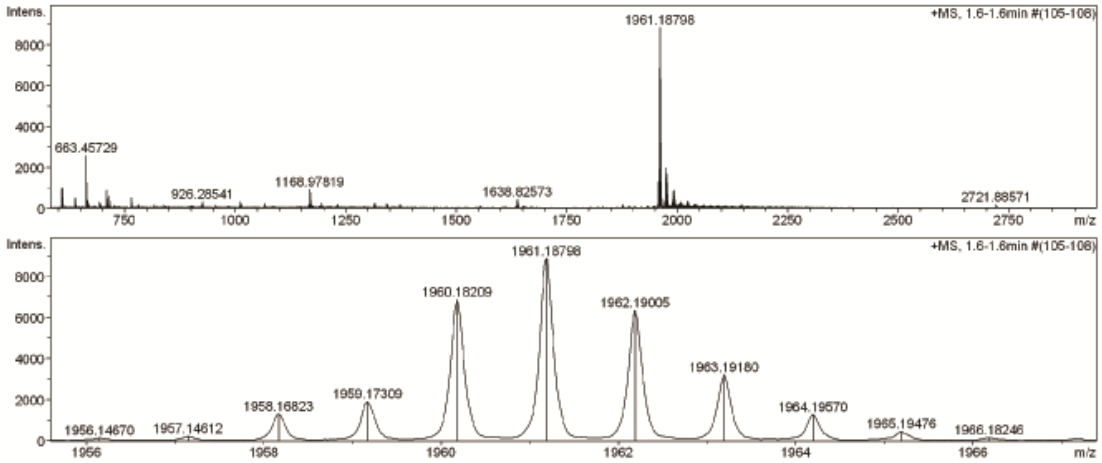

Fig. S9 ESI-MS spectrum and isotopic pattern of compound **F2S**.

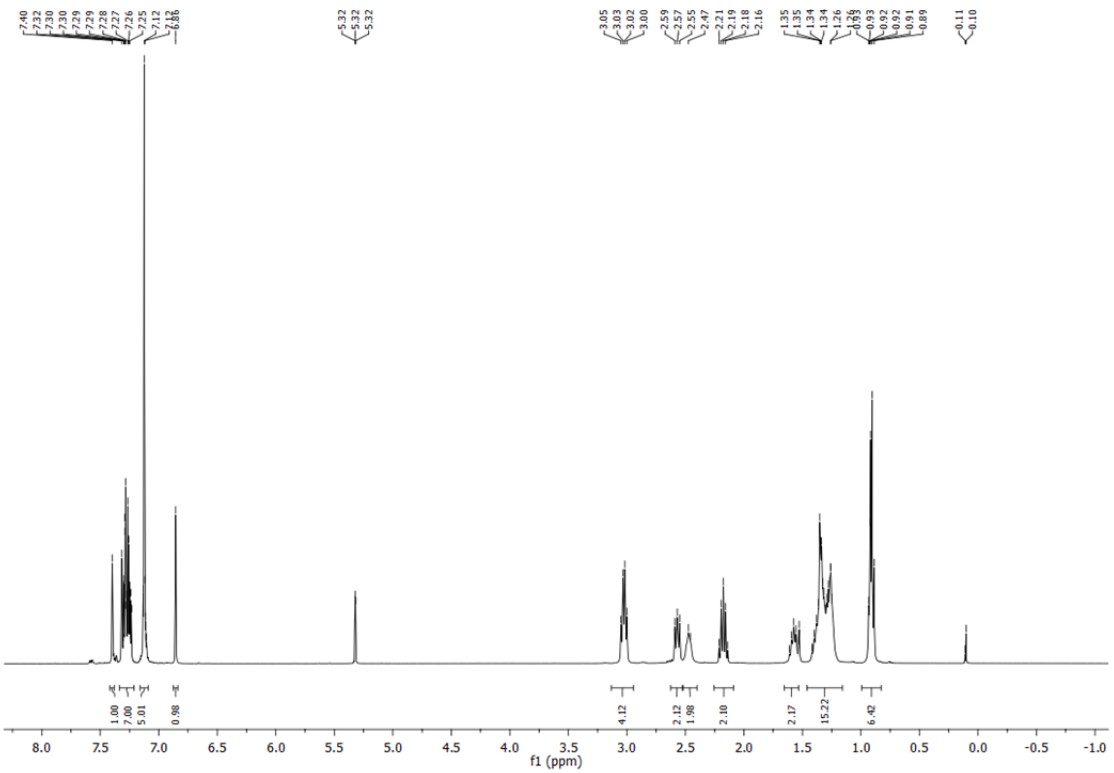

Fig. S10 ^{1}H NMR spectrum of compound **BS** (400 MHz, CD_2Cl_2, 25 °C).

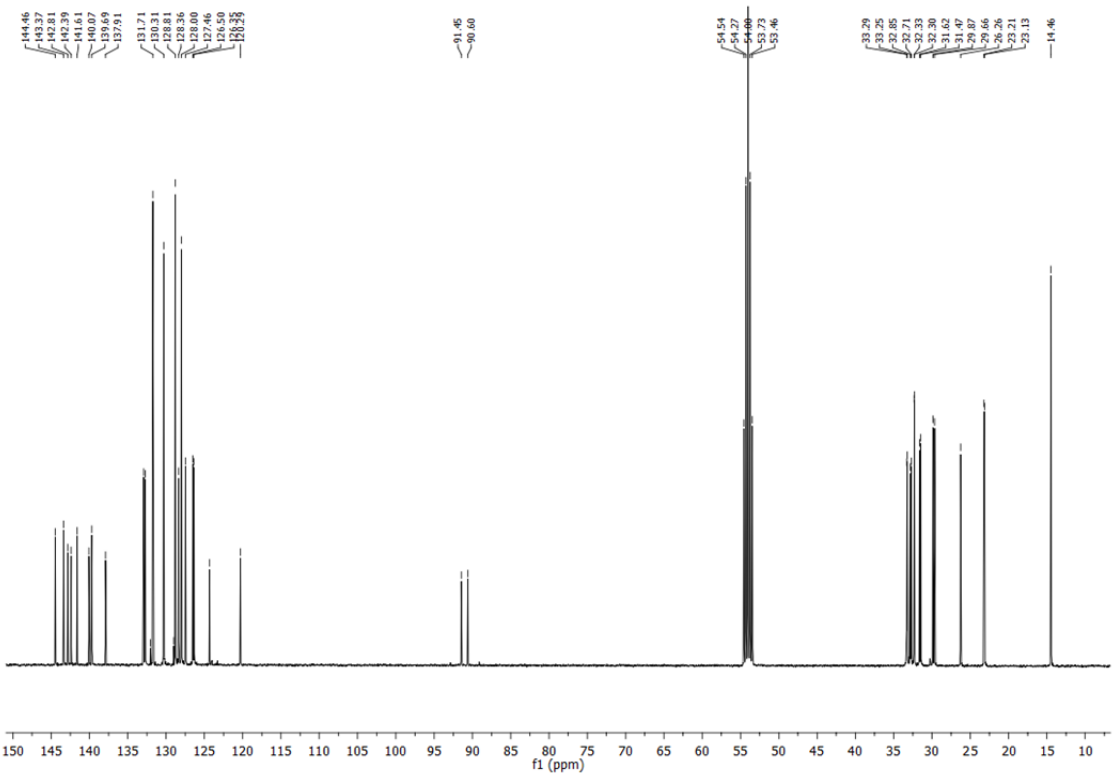

Fig. S11 ^{13}C NMR spectrum of compound **BS** (101 MHz, CD_2Cl_2, 25 °C).

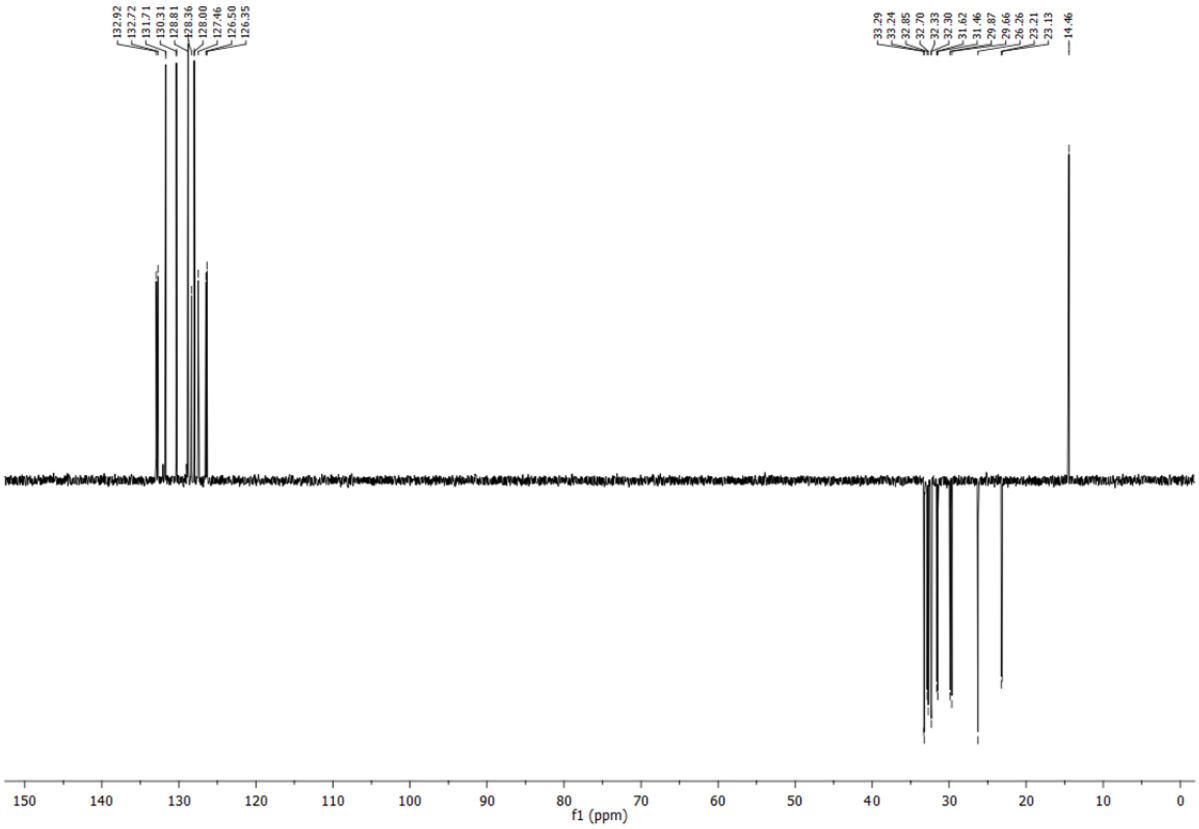

Fig. S12 DEPT-135 spectrum of compound **BS** (101 MHz, CD_2Cl_2, 25 °C).

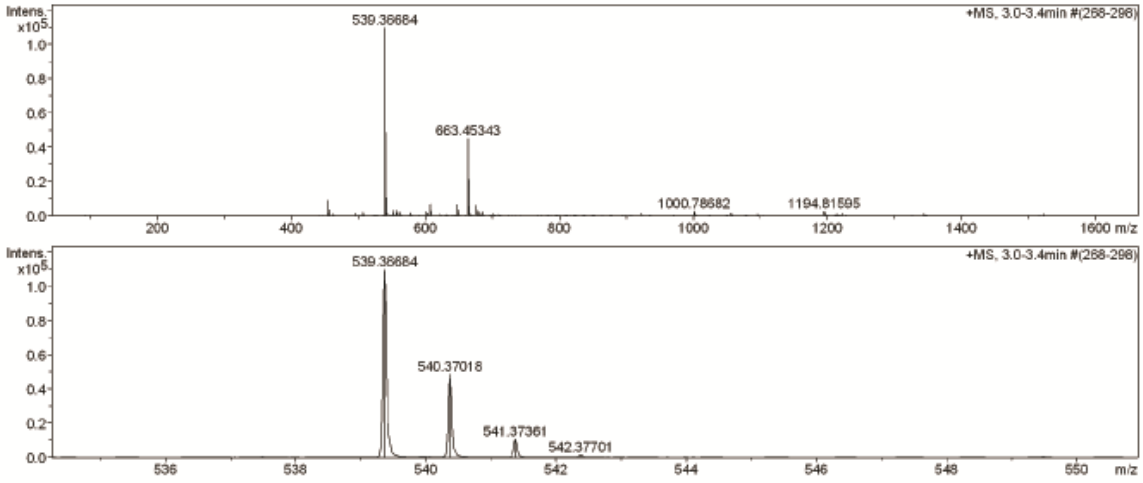

Fig. S13 ESI-MS spectrum and isotopic pattern of compound **BS**.

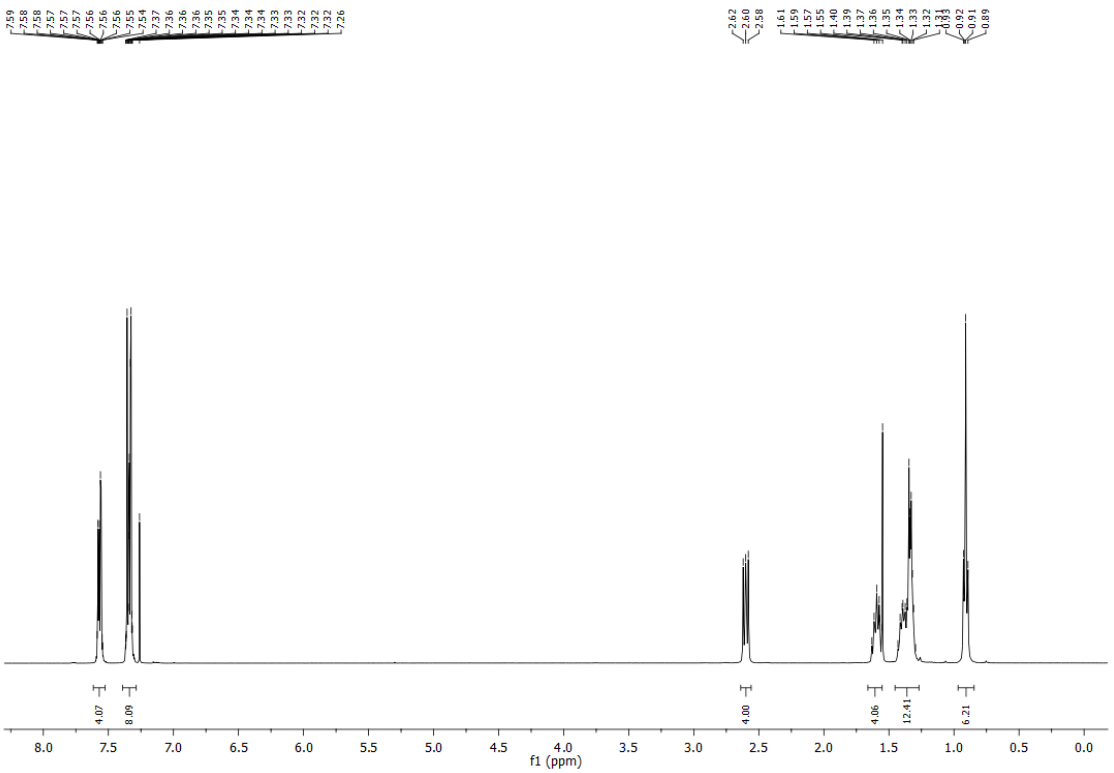

Fig. S14 ^{1}H NMR spectrum of compound **B** (400 MHz, $CDCl_3$, 25 °C).

6. Structure Elucidation for Determination of PET Driving Forces

To estimate the driving forces ($\Delta G°$) for the photoinduced electron transfer (PET) occurring in folda-dimers **F2** and **F2S** or also related p/n-heterojunction ensembles by Rehm-Weller analysis (see equation 1 in the main text), we applied semiempirical methods for geometry optimizations to reveal distinct insights into the spatial arrangements of our two systems. Based on our earlier studies[S1] we already gained structural insights about **F2** by both more sophisticated DFT-D methods and employed here dispersion-corrected and cost-efficient PM6-DH2[S2,S3] approach. First, we optimized folded and unfolded structures of **F2S** and **F2** (*cf.* Fig. S15) with the MOPAC2012 software[S4] (PM6-DH2). In our evaluation of the PET thermodynamics we used the centroids of the donor and the acceptor moieties to calculate the distances r_{CC}, *i.e.* the centers of the backbone (methyl-substituents instead of *n*-hexyl groups) and of the PBI chromophores (for **F2S** see Fig. S16). As a consequence of the unsymmetric character of **F2S** (and also **F2** in the folded state), two slightly different distances ($\Delta \approx 1$Å) between the donor`s centre and the two PBI units are found and therefore the average values are given in Table S1. By comparing these values we see that the values for **F2S** and **F2** are identical in their folded and unfolded states. Thus, the distance (*r*)-related term in our analysis has no impact on the differences in

driving force for the two backbones which is entirely determined by their different oxidation potential. For the estimation of the driving force for the PET process we calculated separately the average ΔG° value for both folded and unfolded states for both folda-dimers based on the average distance-related term. Despite of the 1.9 Å difference in distance, the difference in $\Delta G°$ between folded and unfolded state is essentially negligible. Moreover, as the PBI acceptor's reduction potential of -1.04 V is not influenced by the backbone (the 0.02 V difference for **F2** in Table 2 has been ignored because this difference compared to **F2S**, **M1** and **M2** appears rather to relate to the experimental uncertainty) and the same intersection points (E_{00}) for the PBI systems are used here, the only varying parameter is the oxidation potential of the donor. Accordingly, in our analysis the strongest impact originates from the exchange of the backbone fragment in terms of oxidation potential (**BS** is easier to oxidize).

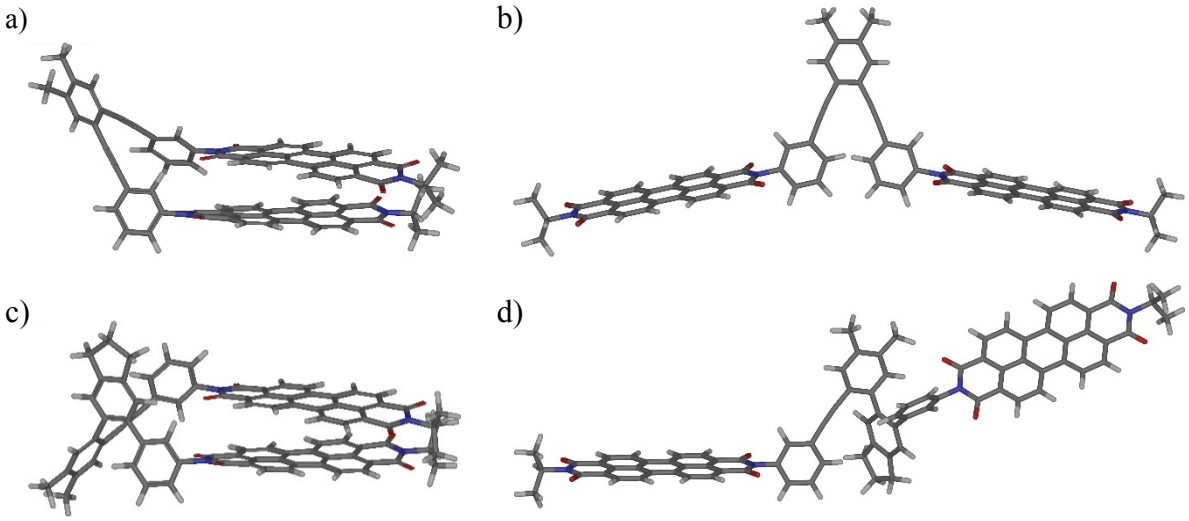

Fig. S15 Geometry optimized structures (with PM6-DH2) of a), b) **F2** and c), d) **F2S** in their folded (left images) and unfolded states (right images).

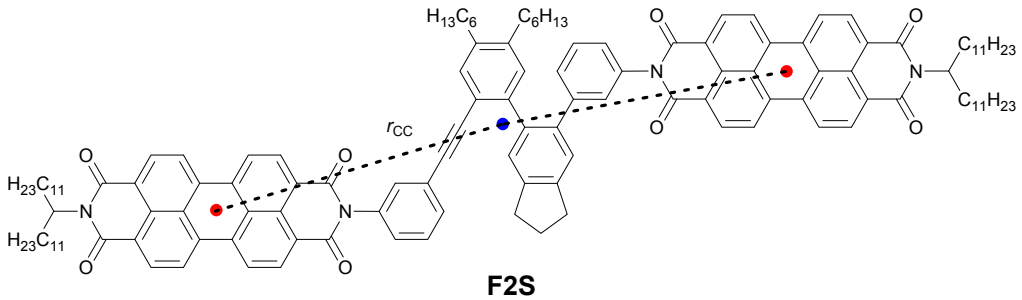

Fig. S16 Distances r_{CC} in **F2S** used for evaluation of the driving force $\Delta G°$ of the electron transfer process. The centroids of the backbone (blue) and of the PBI moieties (red) are indicated in the structure.

Table S1 Determined distances r_{CC}[a] of geometry optimized structures (with PM6-DH2) of **F2** and **F2S** and calculated driving forces for PET.

Cmpd.	State	r_{CC} [Å]	$\Delta G°$ [eV]
F2	folded	10.6	–0.15
	unfolded	12.5	–0.12
F2S	folded	10.6	–0.22
	unfolded	12.5	–0.20

[a] Average for the two distances measured as shown in Fig. S16.

7. Further References

(S1) B. Fimmel, M. Son, Y. M. Sung, M. Grüne, B. Engels, D. Kim and F. Würthner, *Chem. Eur. J.*, 2015, **21**, 615.
(S2) J. Řezáč, J. Fanfrlík, D. Salahub and P. Hobza, *J. Chem. Theory Comp.*, 2009, **5**, 1749.
(S3) M. Korth, M. Pitoňák, J. Řezáč and P. Hobza, *J. Chem. Theory Comp.*, 2010, **6**, 344.
(S4) MOPAC2012, James J. P. Stewart, Stewart Computational Chemistry, Colorado Springs, CO, USA, http://OpenMOPAC.net (2012).